Neutron-polarization-analysis study of the spin structure of Cu-Mn spin-glasses

J. W. Cable
Solid State Division, Oak Ridge National Laboratory, Oak Ridge, Tennessee 37830

S. A. Werner
Department of Physics, University of Missouri at Columbus, Columbus, Missouri 65201

G. P. Felcher
Materials Science and Technology Division, Argonne National Laboratory, Argonne, Illinois 60439

N. Wakabayashi*
Solid State Division, Oak Ridge National Laboratory, Oak Ridge, Tennessee 37830

(Received 4 April 1983)

Neutron-polarization-analysis measurements as well as unpolarized neutron measurements were made of the diffuse scattering from single-crystal Cu-Mn alloys to determine the atomic and spin pair correlations for this spin-glass system. The results show the presence of a spin modulation with a period that varies continuously in terms of the edge of the fcc crystal cell from $6a_0$ at 5 at. % Mn to about $3a_0$ 25 at. % Mn. The correlation length associated with this modulation is about $6a_0$ at all concentrations. Coexistent with these large modulated regions are smaller regions in which the spin correlations are determined by the atomic short-range order and which have net ferromagnetic moments. The interactions between these ferromagnetic and modulated regions are undoubtedly an essential element in understanding the complicated magnetic behavior of this spin-glass system.

INTRODUCTION

The Cu-Mn alloy system is regarded as the prototype of spin-glass behavior. This system has attracted considerable attention in magnetism for a very long time.[1-6] Below a concentration-dependent and fairly well-defined temperature T_f, the spins are believed to freeze in random orientations without long-range order. There are remanent and relaxation-time effects below T_f which indicate energy minima in configuration space separated by some type of anisotropic energy barrier.[4] Despite intense experimental and theoretical effort over the past few years, fundamental questions such as the nature of the freezing process and the origin of the energy barriers remain unresolved. Part of the difficulty in developing an adequate theory is a lack of information on the microscopic spin structure of any spin-glass system.

Murani and co-workers[7-13] have studied the spin dynamics of Cu-Mn alloys using neutron scattering methods with a wide range of energy-resolution conditions. They found ferromagnetic spin pair correlations with a broad spectrum of relaxation times and suggested a dynamic, nonequilibrium, freezing process involving ferromagnetic clusters. The physical connection of these neutron experiments with the recent ESR experiments of Schultz *et al.*[14,15] and the triad dynamics theories of Halperin and Saslow[16-18] have not yet been made. Several quasielastic neutron diffuse scattering studies have been reported[3,19-25] on the correlations of the spins in Cu-Mn. In this system, that crystallizes in a fcc structure for a manganese concentration up to 83 at. %, some degree of chemical short-range order is always present, as evidenced by a diffuse peak at $(1\,0\,\frac{1}{2})$. The earlier neutron measurements, in which the scattering of magnetic and nuclear origin were not separated directly, reached conflicting conclusions about the origin of the diffuse peak at $(1\,0\,\frac{1}{2})$ and the sign of the nearest-neighbor spin pair correlation. It was only by the application of the polarization-analysis technique that Davis, Burke, and Rainford[20] were able to show conclusively that this peak has both nuclear and magnetic components and that the magnetic short-range order parameters (spherically averaged) are negative for first neighbors and positive for second neighbors. In this paper, we describe recent neutron-polarization-analysis results[26] which reveal two distinct types of spin correlations for the Cu-Mn alloys. There are prominent features in the diffuse scattering which were not observed in the earlier neutron studies and which show the presence of incommensurate, long-wavelength modulations that persist over large distances. In addition, there are ferromagnetic correlations over shorter distances which are directly associated with the atomic short-range order. The interactions between these small ferromagnetic regions and the larger modulated regions are undoubtedly an essential ingredient in understanding the unusual magnetic behavior of this spin-glass system.

EXPERIMENT

The measurements were made on Cu-Mn single crystals containing 5, 10, 15, and 25 at. % Mn. The crystals were grown by the Bridgman technique under argon pressure starting from high-purity copper and manganese powders. The crystals were initially annealed by cooling them from 400 to 190 °C over the period of 20 d. These samples were

prepared in 1970; further aging occurred over the years at room temperature. Prior to the measurements, the samples were annealed for a month at 100 °C.

The reason for performing the experiment on well-annealed samples was the following. From the previous scattering measurements it appeared that the basic features of the short-range order remain unaltered upon annealing, in the sense that the maxima of the diffuse peaks remain at the same positions and their relative strength remains unchanged; while their absolute peak intensity may change as well as their width. However, the diffuse peaks have been found in all samples, even in those most drastically quenched or mechanically deformed but still retaining sufficient crystallinity to be amenable to scattering analysis. The thermal treatment affects even less our relatively large ($\sim\frac{2}{3}$-cm^3) single crystals, for which the width of the fcc Bragg reflections is less than 1°. Subsequent quenching on some of our samples indicated only a modest reduction of the short-range order with no significant change of the spin correlations that will be described; no new information was retrieved in these intrinsically more unstable samples. For the measurements described here, not only the samples were well annealed, but all the tests were conducted at a temperature not exceeding 300 K, which is, however, much higher than the temperature of magnetic freezing (reported[6] to be 27 and 100 K for the extremes of the concentration range of our samples).

In the polarization-analysis measurements the polarization of the scattered neutrons was defined by a *Co*Fe analyzer while the incident neutrons were polarized alternately parallel and antiparallel to a horizontal guide field of 20 mT directed parallel to the scattering vector. This allowed separate determinations of cross sections for which the neutron spin was either flipped or unaltered during the scattering. In this geometry, the nuclear scattering occurs without spin flip while the magnetic scattering occurs[20] with spin flip.

The observed nuclear and magnetic cross sections are illustrated by Fig. 1 where the data for the 25 at. % Mn alloy at 10 K are presented as intensity contours in a (010) reciprocal-lattice plane. The nuclear scattering shown in Fig. 1(a) exhibits broad diffuse peaks at $(1,0,\frac{1}{2})$ and at other symmetry-related positions. The magnetic scattering shown in Fig. 1(b) has intensity distributed around (000) and $(1\,0\,\frac{1}{2})$ but the most prominent features are the relatively sharp peaks at $(1,0,\frac{1}{2}\pm\delta)$ and other symmetry-related positions. The positions of these peaks indicate that the modulation of the spin correlations has a period which is long compared with the edge of the crystal cell ($\sim$3.7 Å), while their widths show that this modulation persists over appreciable distances.

These peaks become broader and lower with increasing temperature as illustrated by Fig. 2 which shows the magnetic cross section for Cu—25 at. % Mn measured along the [001] direction from (100) to (101) at the temperatures indicated. The solid curves are least-squares fits to a constant background plus three Gaussian peaks, each of which is described by parameters representing the peak height, peak position, and halfwidth. The peak positions

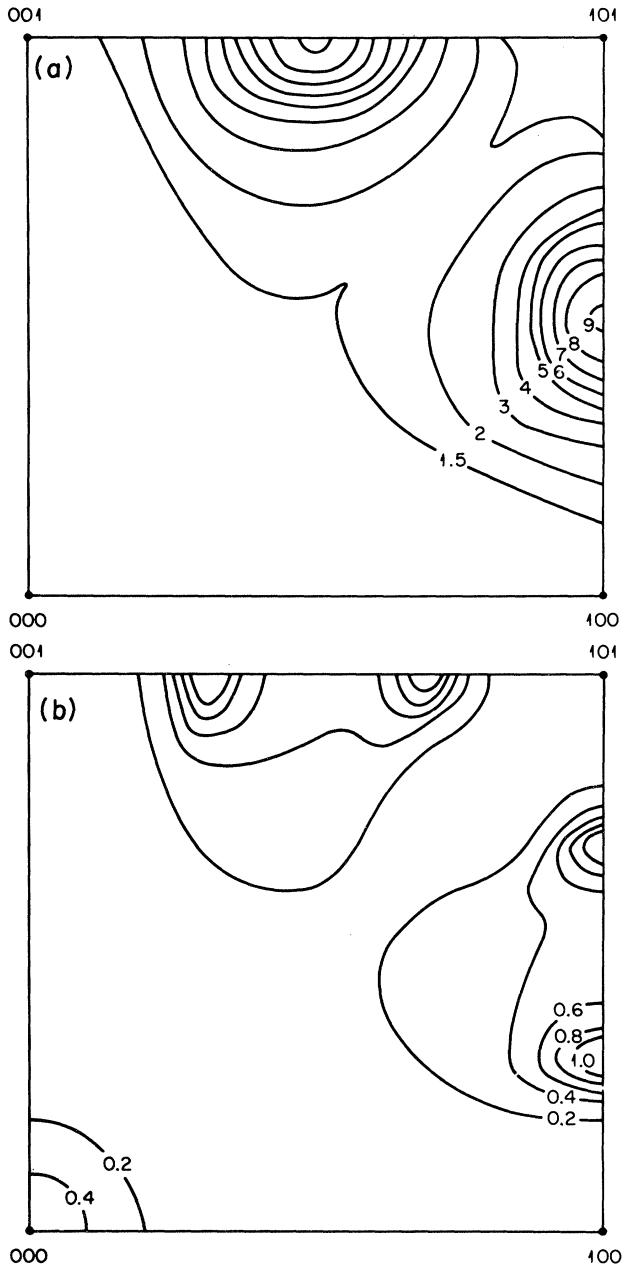

FIG. 1. (a) Non-spin-flip or nuclear and (b) spin-flip or magnetic cross sections for the Cu—25 at. % Mn alloy at 10 K. Intensity contours are in $S(\vec{K})$ units in (a) and in units of barns steradian^{-1} atom^{-1} in (b).

($\zeta=0.31\times2\pi/a_0$, $0.50\times2\pi/a_0$, and $0.69\times2\pi/a_0$) and the halfwidth of the central peak ($\Gamma=0.21\times2\pi/a_0$) are temperature independent while the other parameters show the temperature dependence displayed in Fig. 3. In the upper half of this figure, the open and solid points represent the $(1,0,\frac{1}{2}\pm\delta)$ and $(1\,0\,\frac{1}{2})$ peak heights, respectively. The shaded rectangle at the highest temperature represents both peak heights and reflects the uncertainty in resolving the 292-K data into three peaks. Nevertheless, the magnetic correlations are clearly breaking up at

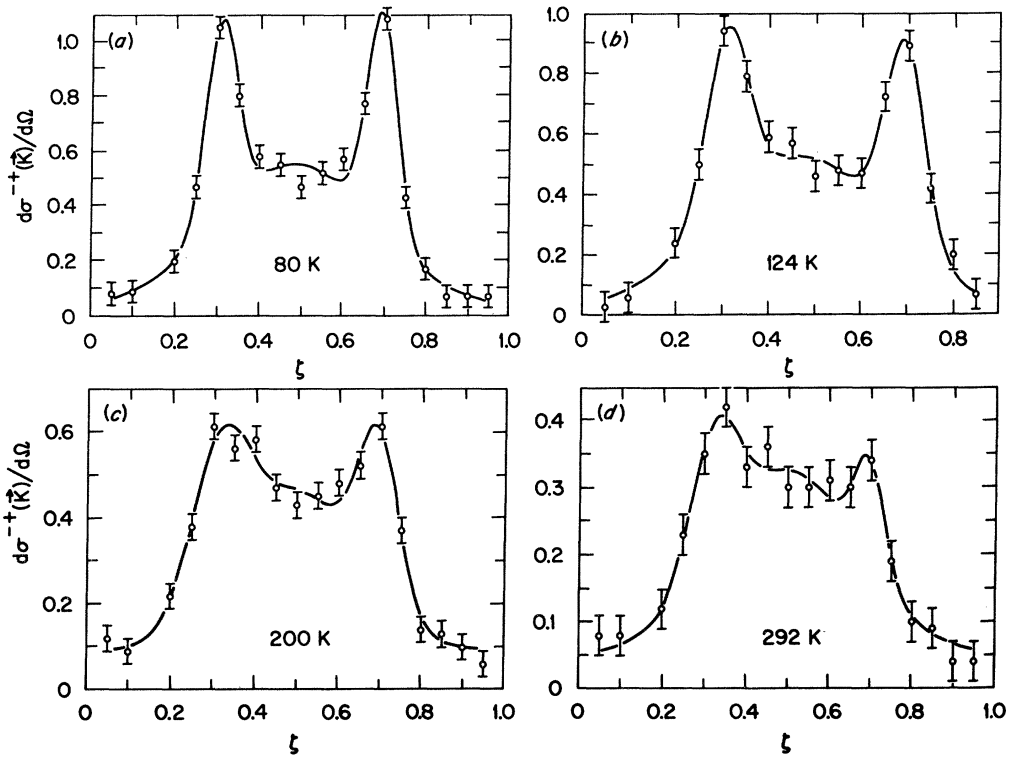

FIG. 2. Magnetic cross section for Cu—25 at. % Mn along $(1\,0\,\zeta)$ at elevated temperatures.

the higher temperatures and an approximate extrapolation suggests that the spins would become completely uncorrelated in the (350—400)-K region. There is no apparent discontinuity for either set of intensity data at the freezing temperature of 100 K. The temperature dependence of the average $(1,0,\frac{1}{2}\pm\delta)$ halfwidth is shown in the lower half of the figure. There is a gradual increase in Γ, i.e., a decrease in the correlation length with increasing temperature. Similar results were obtained for Cu—15 at. % Mn and the temperature-dependent effects are summarized on the right-hand side of Fig. 3.

Only after proving by polarization analysis that the non-spin-flip, or nuclear, cross section remains unchanged over this temperature range, it was possible to decide that

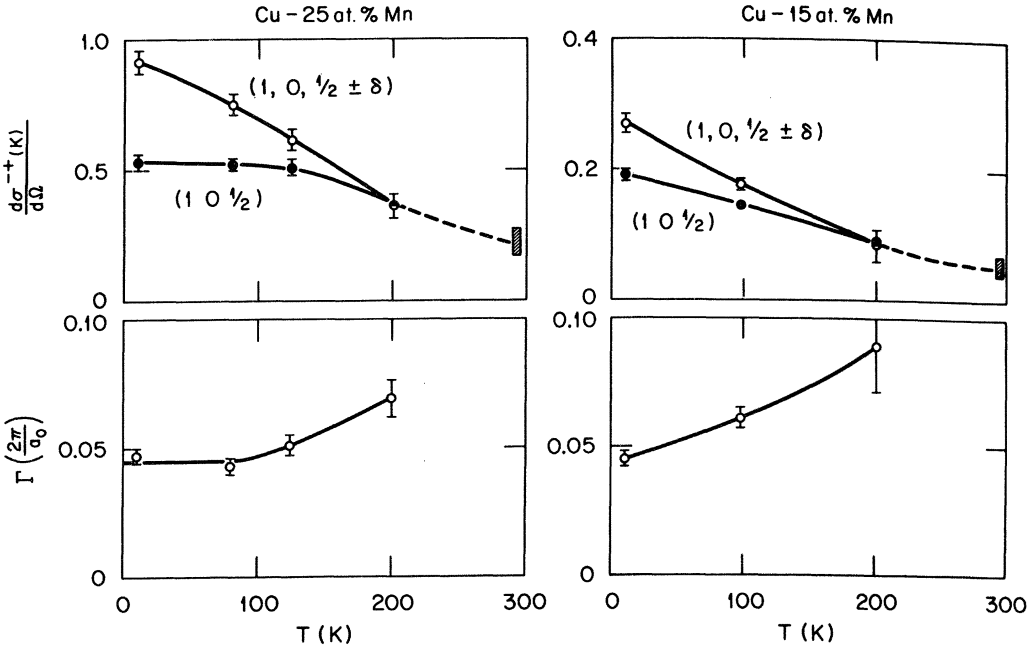

FIG. 3. Temperature dependence of the peak-height intensity at $(1,0,\frac{1}{2})$ and $(1,0,\frac{1}{2}\pm\delta)$ and of the $(1,0,\frac{1}{2}\pm\delta)$ halfwidth for Cu—25 at. % Mn and Cu—15 at. % Mn.

the magnetic and nuclear scattering could be separated simply by taking the difference of the cross sections at the two temperatures. In this more conventional method is sufficient to use unpolarized neutrons, and the elimination of the polarization circuits translates into higher neutron intensities. The temperature-difference method is illustrated in Fig. 4, which shows the difference between cross sections measured at 10 and 295 K for the 15 and 25 at. % Mn alloys. These are only approximate magnetic cross sections because some magnetic scattering remains at 295 K at these high-Mn-concentration levels. Nevertheless, the essential features are the same as for the polarization analysis results (compare with Fig. 6) in spite of a slight difference in the sample environment for the two measurements. While in the case of unpolarized neutrons no magnetic field was applied, in the polarization-analysis technique a modest guide field (20 mT) is required. The identity of the results confirms that the perturbing effects of the guide field on the spin correlations are negligible.

Although both separation techniques were used at all four concentrations, we consider that the polarization-analysis results are better for the 15 and 25 at. % Mn alloys and that the temperature-difference results are better for the two more dilute alloys. Accordingly, our best one-dimensional cross-section data are shown in Figs. 5 and 6. These data were least-squares-fitted to background plus either a single Gaussian for the nuclear cross sections (Fig. 5) or three Gaussians for the magnetic cross sections (Fig. 6). The solid curves in these figures represent these fits and the concentration dependence of the fitting parameters is summarized in Fig. 7. All of the peak-height intensities, which include the backgrounds in this figure, increase approximately with the square of the Mn concentration as indicated by the solid curves in Fig. 7(a). The halfwidth of the $(1,0,\frac{1}{2}\pm\delta)$ peak is independent of concentration with a value of $\Gamma=0.045\times 2\pi/a_0$ while the halfwidths of both the nuclear and magnetic peaks at $(1\,0\,\frac{1}{2})$ are considerably larger and also concentration dependent. The displacement δ of the relatively sharp peaks from $(1\,0\,\frac{1}{2})$ is similar in magnitude and concentration dependence as shown by the solid points in Fig. 7(b).

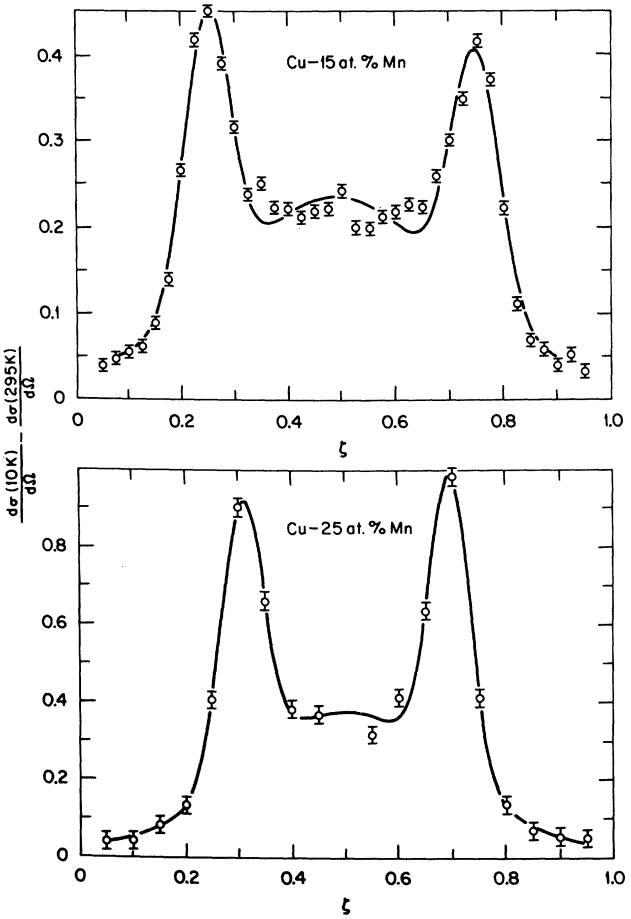

FIG. 4. Temperature-difference (10—295 K) cross sections for Cu—15 at. % Mn and Cu—25 at. % Mn along $(1\,0\,\zeta)$. Compare with the spin-flip cross sections in Figs. 6(c) and (d).

ANALYSIS: NUCLEAR SCATTERING

The non-spin-flip, or nuclear, cross section is given by

$$\frac{d\sigma^{++}}{d\Omega}(\vec{K})=c(1-c)(b_{\mathrm{Mn}}-b_{\mathrm{Cu}})^2 S(\vec{K}) , \tag{1}$$

where $b_{\mathrm{Mn}}=-0.373$, $b_{\mathrm{Cu}}=0.772\times 10^{-12}$ cm, and

$$S(\vec{K})=\sum_{\vec{R}}\alpha(\vec{R})e^{i\vec{K}\cdot\vec{R}} , \tag{2}$$

where the $\alpha(\vec{R})$ are Warren-Cowley short-range order parameters. Since the observed intensity distribution has cubic symmetry, $S(\vec{K})$ can be written in the form

$$S(h_1,h_2,h_3)=\sum_l\sum_m\sum_n \alpha_{lmn}\cos(\pi l h_1)\cos(\pi m h_2)\times\cos(\pi n h_3) , \tag{3}$$

where $\vec{K}=2\pi(h_1\vec{b}_1+h_2\vec{b}_2+h_3\vec{b}_3)$ and $\vec{R}=\frac{1}{2}l\vec{a}_1+\frac{1}{2}m\vec{a}_2+\frac{1}{2}n\vec{a}_3$. In the present analysis, a 20×20 array of the $h_2=0$ data shown in Fig. 2 was Fourier-transformed using the expression

$$A_{ln}\equiv\sum_m\alpha_{lmn}=\frac{1}{V}\sum_{h_1}\sum_{h_3}S(h_1,0,h_3)\cos(\pi l h_1)\cos(\pi n h_3) \tag{4}$$

to obtain the A_{ln} coefficients given in the second column of Table I. Although the observations were limited to a plane, the determination of the three-dimensional short-range-order coefficients α_{lmn} can be attained almost completely. For this orientation, the A_{ln} separate into two independent sets which couple only to the odd- and even-shell α_{lmn}. The A_{ln} appear to have significant values out to A_{52} for the odd shells and to A_{62} for the even shells corresponding to significant α_{lmn} to at least α_{521} (fifteenth shell) and α_{620} (eighteenth shell). This range is no problem for the odd shells where there are sufficient $A_{ln}=\sum_m\alpha_{lmn}$ equations for solution to the twenty-third shell, but does become a problem for the even shell α_{lmn} which are underdetermined beyond the tenth shell. The odd-shell α_{lmn} were determined by the least-squares

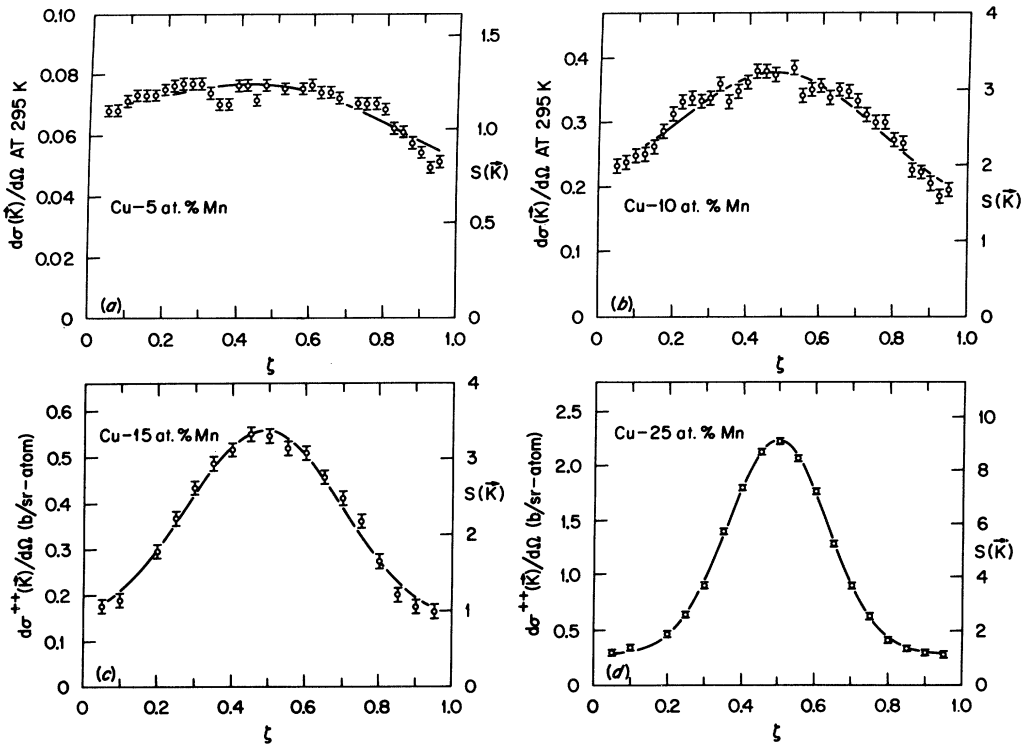

FIG. 5. Nuclear cross sections along (10ζ). Unpolarized-neutron data are shown in (a) and (b) and polarization-analysis results are presented in (c) and (d). $S(\vec{K})$ scales are given on the right-hand side of each figure.

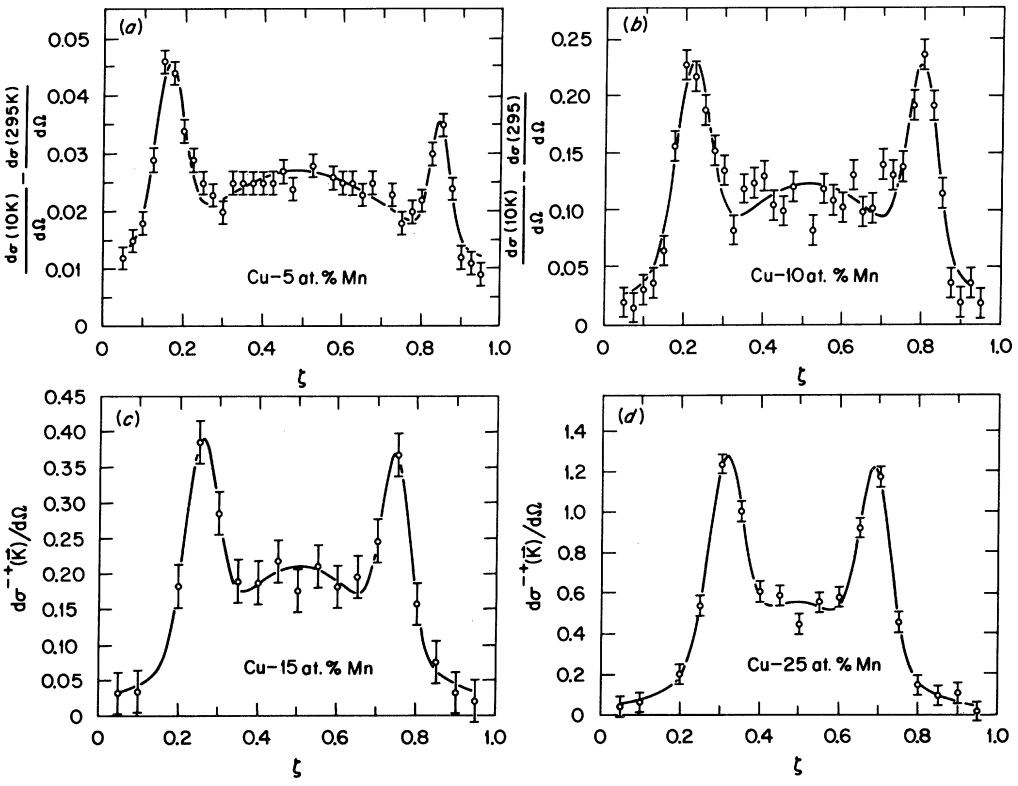

FIG. 6. Magnetic cross sections along (10ζ). Unpolarized-neutron, temperature-difference data appear in (a) and (b), while the 10-K polarization-analysis data are shown in (c) and (d).

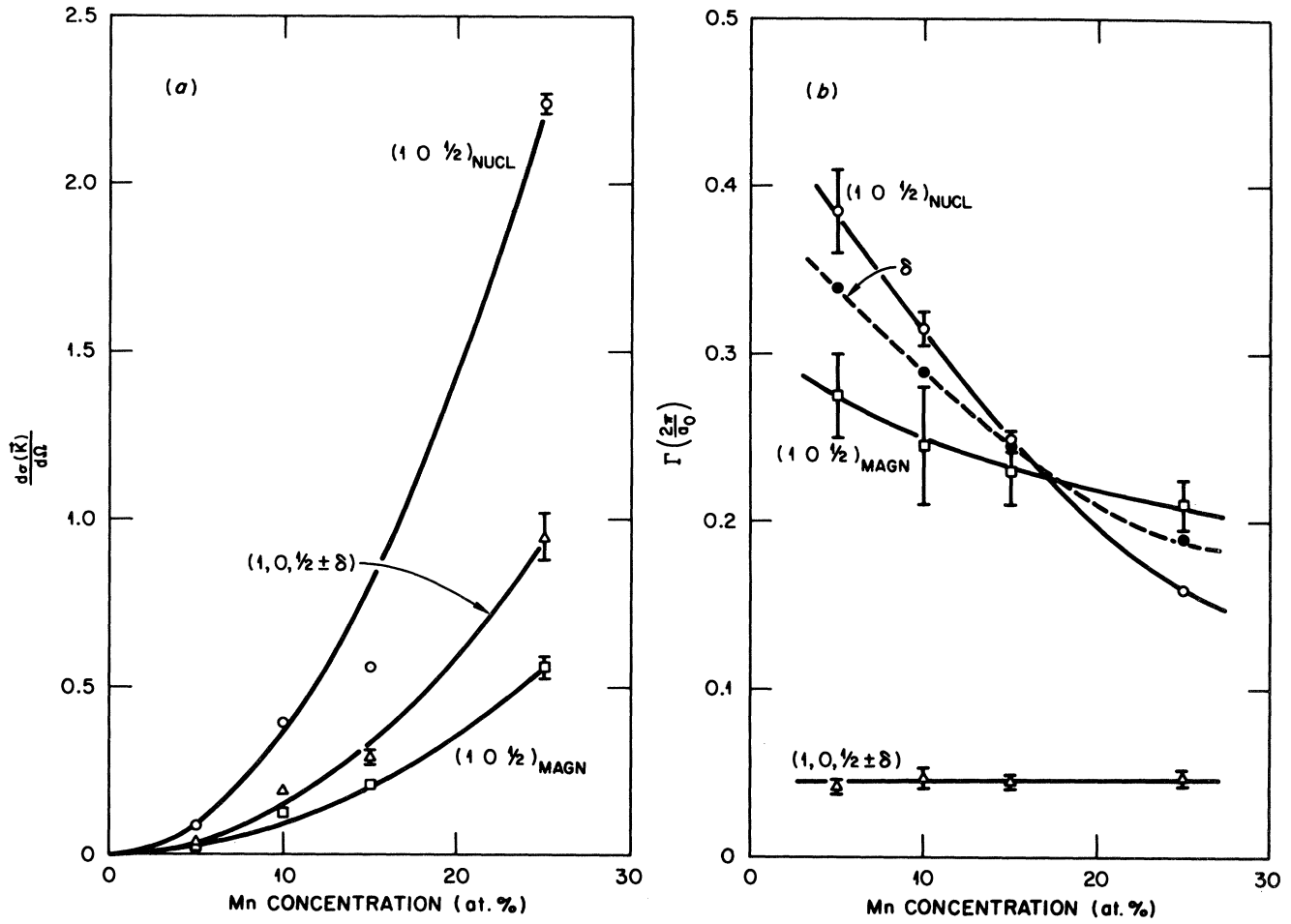

FIG. 7. Concentration dependence of the (a) peak-height intensities and (b) halfwidths of the $(1\,0\,\frac{1}{2})$ and $(1,0,\frac{1}{2}+\delta)$ peaks. Solid points in (b) show the concentration dependence of δ.

method with the assumption that all equidistant α's are equal and the results are given in column five of Table I. These alternate in sign and decrease in magnitude with increasing R. A_{ln} values calculated from these α_{lmn} appear in column three and agree very well with the transformed values. Additional information is needed to solve for the even-shell α_{lmn} and for this we have correlated the odd-shell α_{lmn} with those calculated for long-range-ordered structures damped out over short distances. The best structure and damping is then used to obtain additional relations between the even-shell α_{lmn}.

There are several superlattice structures of the $\langle 1\,0\,\frac{1}{2}\rangle$ family,[27] the simpler of which are the A_2B_2, A_3B, and A_4B tetragonal structures that consist of (201) planes stacked in the sequences *AABB*, *AAAB*, and *AAAAB*. The A_3B and A_4B structures are close to the present stoichiometry and both have been used[21,22,28] as model structures for the short-range order in Cu—25 at.% Mn. However, as Bouchiat *et al.*[29] have noted in their study of Ag-Mn alloys, the A_3B structure produces superlattice peaks at (001) and (110) positions where no diffuse intensity is observed and should not be used to describe the short-range order in either Ag-Mn or Cu-Mn alloys. The A_4B structure does not have this problem but yields α_{lmn} that are out of phase with the observed sign sequence after the ninth shell. The best representation of the observed α_{lmn} is obtained with the A_2B_2 structure which can be described as a composition wave with a modulation wave vector given by

$$\vec{Q}_N = 2\pi(\vec{b}_1 + \tfrac{1}{2}\vec{b}_3)\ . \tag{5}$$

This corresponds to a modulation along the z axis with a period of $2a_0$ with unlike nearest neighbors in the x-y plane. The $\alpha(\vec{R})$ for this tetragonal structure are given by

$$\alpha(\vec{R})_t = \frac{c}{1-c}\cos(\vec{Q}\cdot\vec{R}) + \frac{1-2c}{1-c}\delta_{R0}\ , \tag{6}$$

where the subscript t indicates that the α's are for the tetragonal structure. Equivalent tetragonal domains develop with modulations along the x and y axes and the $\alpha(\vec{R})_t$ must be averaged over domains for comparison with the cubic $\alpha(\vec{R})$ obtained from the data. These cubically averaged α_{lmn} for the odd shells all have a magnitude of $\frac{1}{9}$ and the same sign sequence as that observed.

TABLE I. Atomic short-range order parameters for Cu—25 at. % Mn.

		$A_{ln}=\sum_m \alpha_{lmn}$				
ln	A_{ln} [a]	A_{ln} [b]	lmn	α_{lmn} [c]	α_{lmn} [d]	α_{lmn} [e]
10	−0.426	−0.438	110	−0.124	−0.080	−0.046
11	−0.053	−0.042	211	0.059	0.042	0.027
21	0.264	0.280	310	−0.073	−0.027	−0.021
30	−0.205	−0.212	321	0.061	0.019	0.010
31	0.025	0.005	330	−0.023	−0.020	−0.005
32	0.125	0.142	411		−0.017	
33	−0.008	−0.033	332	0.005	0.001	
41	−0.084	−0.090	510	−0.022	−0.003	
50	−0.064	−0.064	431		−0.002	
51	−0.009	0.018	521	0.020	0.001	
43	−0.044	−0.064	530	−0.010	0.000	
52	0.062	0.050	433		−0.002	
61	0.007	0.010	611	0.005		
53	−0.002	0.000	532			
00	1.936	1.936	000	1.60		
20	−0.028	−0.028	200	0.056	0.061	0.041
22	−0.360	−0.360	220	−0.060	−0.036	−0.016
40	0.208	0.216	222	−0.102	−0.050	−0.043
42	−0.032	−0.020	400	0.104	0.051	0.029
44	0.075	0.074	420	0.028	0.010	0.005
60	0.045	−0.012	422	−0.028	−0.003	
62	−0.051	−0.050	440	0.028	0.006	
			442	0.008		
			600			
			620	−0.010		
			622	−0.020		
			444	0.015		

[a]Fourier-transformed values.
[b]Calculated from α_{lmn}.
[c]Present results.
[d]Reference 28.
[e]Reference 19.

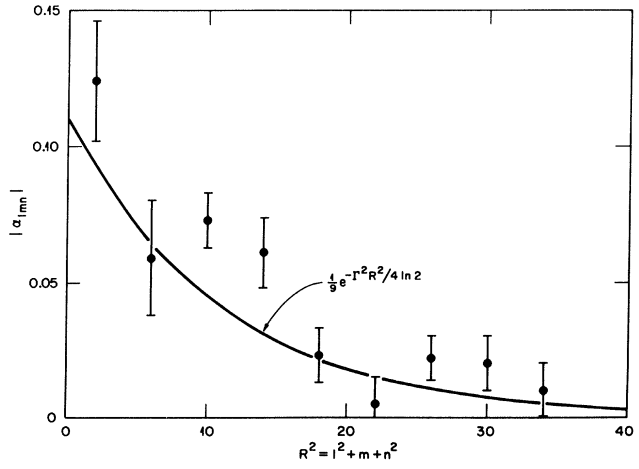

FIG. 8. Magnitude of the odd-shell α_{lmn} vs R^2 for Cu—25 at. % Mn compared to the calculated behavior for the A_2B_2 structure with Gaussian damping. ($\Gamma=0.16\times 2\pi/a_0$.)

Since the Fourier transform of the Gaussian $\exp(-K^2/\sigma^2)$ is a Gaussian of the form $\exp(-\sigma^2R^2/4)$, the damping factor can be taken from the observed halfwidth Γ, where $\sigma^2=\Gamma^2/\ln 2$. This model calculation is compared with the observations in Fig. 8 where the open points represent the magnitude of the odd-shell α_{lmn} and the solid curve is the Gaussian $\exp(-\Gamma^2R^2/4\ln 2)$ with the observed $\Gamma=0.16\times 2\pi/a_0$ normalized to $\frac{1}{9}$ at $R=0$. This damped A_2B_2 model gives a reasonable representation of the data and was used in solving for the even-shell α_{lmn} which are given in the lower half of Table I. These yield A_{ln} in good agreement with the transformed values except for A_{60}. The present α_{lmn} are compared with those previously determined[19,28] for the same composition in the last three columns of Table I. Our samples appear more highly ordered than the other two samples but the signs of the $\alpha(R)$ are in complete agreement for all shells. Here, a negative (positive) $\alpha(R)$ indicates a preference for unlike (like) neighbors, so the observed sequence shows that Mn atoms prefer Cu first neighbors and Mn second neighbors. Since first neighbors presumably interact antiferromagnetically and second neighbors interact ferromagnetically, short-range order

should enhance the ferromagnetic properties of the system. There is abundant experimental evidence[2,5,30–33] that this is indeed the case.

ANALYSIS: MAGNETIC SCATTERING

The paramagnetic cross section is known to be inelastic but the observed[7–13] energy transfers are only about 1 meV. In this experiment, the incident energy was 72 meV with an energy resolution of 2.5 meV halfwidth at the half maximum so that the quasielastic approximation should be valid. In this approximation, the paramagnetic cross section is[34]

$$\frac{d\sigma^{-+}}{d\Omega}(\vec{K})=\left[\frac{e^2\gamma}{mc^2}\right]^2[f(\vec{K})]^2\sum_{\alpha,\beta}(\delta_{\alpha\beta}-\hat{K}_\alpha\hat{K}_\beta)\times\sum_{\vec{R}}\langle s^\alpha_{\vec{R}}s^\beta_{\vec{0}}\rangle e^{i\vec{K}\cdot\vec{R}}\ , \tag{7}$$

where $f(\vec{K})$ is the magnetic form factor, α and β denote Cartesian components of the spin, and $\langle s^\alpha_{\vec{R}}s^\beta_{\vec{0}}\rangle$ is the quasistatic spin-spin correlation.

The magnetic cross sections cannot be simply Fourier-transformed to obtain magnetic short-range order parameters because of the long correlation lengths associated with the $(1,0,\frac{1}{2}\pm\delta)$ peaks. Instead, we calculate the cross sections for assumed spin correlation models and compare directly with the observed cross sections. In this calculation, the fact that only the Mn atoms have spins is taken into account by introduction of the site occupation operator $p_{\vec{R}}$, which counts the number (0 or 1) of Mn atoms at $\vec{R}$. The spin correlation is then

$$\langle s_{\vec{R}}s_{\vec{0}}\rangle=\langle p_{\vec{R}}p_{\vec{0}}s_{\mathrm{Mn}}(\vec{R})s_{\mathrm{Mn}}(\vec{0})\rangle\ , \tag{8}$$

and the Mn-Mn atom pair correlation is

$$\langle p_{\vec{R}}p_{\vec{0}}\rangle=c^2+c(1-c)\alpha(\vec{R})\ . \tag{9}$$

As can be seen in Fig. 7, the magnetic and nuclear peaks at $(1\,0\,\frac{1}{2})$ have intensities that are proportional and also have similar concentration-dependent halfwidths. The spin correlations responsible for the $(1\,0\,\frac{1}{2})$ diffuse peaks therefore have nearly the same range and relative magnitudes as the atom pair correlations. There are two obvious types of spin correlation that will produce this peak. One is a ferromagnetic correlation within the short-range-ordered regions and the other is an antiferromagnetic correlation with the same modulation wave vector as for the composition wave. For the ferromagnetic case, the Mn-Mn spin correlation is just s^2_{Mn} and the total correlation becomes

$$\langle s_{\vec{R}}s_{\vec{0}}\rangle=s^2_{\mathrm{Mn}}[c^2+c(1-c)\alpha(\vec{R})]\ . \tag{10}$$

This produces peaks at the fundamental reciprocal-lattice vectors $\vec{G}$, and also at $\vec{K}=\vec{G}\pm\vec{Q}_N$. The ferromagnetism can be confined to the short-range-ordered regions by multiplying the c^2 term by a damping factor $\exp(-\Gamma^2R^2/4\ln 2)$. Both sets of peaks will then have the same halfwidth, Γ. However, the peaks at $\vec{G}$ are more intense since they are derived from the entire sample while the peaks at $\vec{G}\pm\vec{Q}_N$ arise only from the z-axis domains. This ferromagnetic correlation seems to describe the low-Mn-concentration region (less than 10 at.% Mn) where the observed cross sections are larger near $\vec{G}$ than at $\vec{G}\pm\vec{Q}_N$. However, inspection of Fig. 1(b) shows that this is not the case at 25 at.% Mn, so we must consider the alternate antiferromagnetic correlation for the more concentrated alloys. This can be expressed in terms of the Mn-Mn atom pair correlation which, for $R\neq 0$, fluctuates about the average of c^2 between the limits of $2c^2$ and zero. If for simplicity the manganese spins are visualized as collinear, their correlation must fluctuate about zero between the limits of $\pm s^2_{\mathrm{Mn}}$. If we assume a positive (negative) correlation when $\langle p_{\vec{R}}p_{\vec{0}}\rangle$ is larger (smaller) than c^2, then, for $\vec{R}\neq\vec{0}$,

$$\langle s_{\mathrm{Mn}}(\vec{R})s_{\mathrm{Mn}}(\vec{0})\rangle=s^2_{\mathrm{Mn}}\left[\frac{\langle p_{\vec{R}}p_{\vec{0}}\rangle}{c^2}-1\right]\ . \tag{11}$$

This relationship between the Mn-Mn spin pair and atom pair correlations is shown schematically in Fig. 9. From Eqs. (8), (9), and (11), the total spin correlation at all $\vec{R}$ becomes

$$\langle s_{\vec{R}}s_{\vec{0}}\rangle=s^2_{\mathrm{Mn}}[\,c(1-c)\alpha(\vec{R})+(1-c)^2\alpha^2(\vec{R})-(1-2c)\delta_{R0}]\ . \tag{12}$$

For z-axis tetragonal domains with the spins assumed to lie in the x-y plane, the cross section is then

$$\frac{d\sigma^{-+}}{d\Omega}(\vec{K})=\left[\frac{e^2\gamma}{mc^2}\right]^2[f(\vec{K})]^2\frac{1+K_z^2}{2}\times s^2_{\mathrm{Mn}}[\,c(1-c)S(\vec{K})+(1-c)^2T(\vec{K})-(1-2c)]\ , \tag{13}$$

where $S(\vec{K})$ is defined by Eq. (2) and

$$T(\vec{K})=\sum_{\vec{R}}\alpha^2(\vec{R})e^{i\vec{K}\cdot\vec{R}}\ . \tag{14}$$

The $S(\vec{K})$ term is the same as in the nuclear cross section and peaks at $\vec{K}=\vec{G}\pm\vec{Q}_N$ while the $T(\vec{K})$ term peaks at $\vec{K}=\vec{G}$ and $\vec{G}\pm2\vec{Q}_N$. The latter are broader and less intense than the $S(\vec{K})$ peaks. This peaking at the funda-

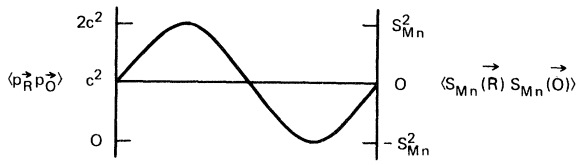

FIG. 9. Schematic representation of the Mn-Mn atom pair and spin pair correlations in the [201] direction.

mental positions reflects the ferromagnetic character of these short-range-ordered regions, which results from the phasing of the spin pair and atom pair correlations. This phasing places more than the average number of Mn atoms in positive-spin regions and less than the average number of Mn atoms in the negative-spin regions. The result is a net ferromagnetism and diffuse peaks at all $\vec{G}$. We will therefore refer to this correlation as short-range ferromagnetic order even though it arises from an antiferromagnetic Mn-Mn correlation. The ferromagnetic correlation expressed by Eq. (10) and the antiferromagnetic correlation given in Eq. (12) both contain the term $c(1-c)\alpha(\vec{R})$ which also occurs in the atom pair correlation of Eq. (9). It is the Fourier transform of this term, $S(\vec{K})$, that gives rise to the peak at $(1\,0\,\frac{1}{2})$ in both the magnetic and nuclear cross sections. We therefore extracted s_{Mn} values from the ratio of the observed magnetic and nuclear cross sections at $(1\,0\,\frac{1}{2})$ by using Eqs. (1) and (13). The values obtained are given in Table II and are near the expected value of $S=2$ at all concentrations.

In considering the $(1,0,\frac{1}{2}\pm\delta)$ peaks that arise from the long-period modulations, we note that the data do not define the type of modulation. This could be sinusoidal, as in a spiral configuration, or square wave, as in an antiphase domain. The scattering from these and from other intermediate-type modulations is quite similar. In the following calculations we use a spiral model for simplicity even though this configuration is not established from the data. In any event, the spin values obtained are not very sensitive to the type of modulation.

The data show that there is a modulation with a wave vector

TABLE II. Magnetic parameters for Cu-Mn alloys.

c	$\frac{1}{2}-\delta$	s_{Mn} [a]	s_{Mn} [b]
0.05	0.16	1.94	1.18
0.10	0.21	1.82	1.23
0.15	0.25	1.96	1.19
0.25	0.31	1.67	1.36

[a]From $(1\,0\,\frac{1}{2})$ intensities and Eq. (13).

[b]From $(1,0,\frac{1}{2}\pm\delta)$ intensities and Eq. (18).

$$\vec{Q}_M=2\pi[\vec{b}_1+(\tfrac{1}{2}-\delta)\vec{b}_3]\,. \tag{15}$$

This corresponds to a modulation along the z axis with a period of $a_0/(\frac{1}{2}-\delta)$ and with the condition that first-neighbor spins in the x-y plane are oppositely aligned. Equivalent tetragonal domains are required along the x and y axes. In a spiral configuration with the spins in the x-y plane normal to the tetragonal z axis, the spin components at $\vec{R}$ are

$$s^x_{\vec{R}}=p_{\vec{R}}\,s_{\mathrm{Mn}}\cos(\vec{Q}_M\cdot\vec{R}+\phi) \tag{16}$$

and

$$s^y_{\vec{R}}=p_{\vec{R}}\,s_{\mathrm{Mn}}\sin(\vec{Q}_M\cdot\vec{R}+\phi) \tag{17}$$

The corresponding cross section is

$$\frac{d\sigma^{-+}}{d\Omega}(\vec{K})=\left[\frac{e^2\gamma}{mc^2}\right]^2[f(\vec{K})]^2\frac{1+K_z^2}{4}s_{\mathrm{Mn}}^2\left[c^2\sum_{\vec{R}}e^{i(\vec{K}\pm\vec{Q}_M)\cdot\vec{R}}+c(1-c)S(\vec{K}\pm\vec{Q}_M)\right], \tag{18}$$

where the first term gives Bragg peaks at $\vec{K}=\vec{G}\pm\vec{Q}_M$ and the second term gives broad peaks at $\vec{K}=\vec{G}\pm\vec{Q}_N\mp\vec{Q}_M$. Of course, Bragg peaks are not observed because the spiral order persists only over short distances. Nevertheless, the volume integrals of the calculated and observed peaks can be compared to obtain s_{Mn} values. This requires some assumptions since two-dimensional data were obtained only for the 25-at.% Mn alloy. If Γ_i is defined as the halfwidth in the reciprocal-lattice direction $\vec{b}_i$, then the observed halfwidths for Cu—25 at.% Mn are $\Gamma_1=0.105$ and $\Gamma_3=0.045\times2\pi/a_0$ at $(1,0,\frac{1}{2}-\delta)$ and $\Gamma_1=\Gamma_3=0.045\times2\pi/a_0$ at $(1,0,\frac{1}{2}+\delta)$. These diffuse peaks are therefore ellipsoidal with their major axes parallel to $\vec{b}_1$ and $\vec{b}_2$, respectively. The reciprocal-lattice representation of the relative orientations of these diffuse peaks is shown schematically in Fig. 10. Since Γ_3 is independent of concentration [Fig. 7(b)], we assume that the same shape and widths apply at all four concentrations. The volume integral of the observed cross section is then $d\sigma/d\Omega(0)\sigma_1\sigma_2\sigma_3\pi^{3/2}\epsilon$ where $d\sigma/d\Omega(0)$ is the peak-height intensity, $\sigma_i^2=\Gamma_i^2/\ln 2$, and ϵ is a correction factor for the vertical resolution. For the present resolution conditions ($0.012\times2\pi/a_0$ horizontal and $0.040\times2\pi/a_0$ vertical), we obtain $\epsilon=1.31$. The volume integral is compared with the cross section calculated from Eq. (18) using a Bragg-peak volume integral of $4(2\pi/a_0)^3$. By taking into account that only $\frac{1}{6}$ of the crystal volume contributes to each $(1,0,\frac{1}{2}\pm\delta)$-type peak, we obtain the s_{Mn} values listed in Table II. These are approximately the same at each concentration but are smaller than those derived from the ferromagnetic short-range order. This is not surprising because the spiral order is locally perturbed by the ferromagnetic short-range order. This perturbation is not enough to destroy the coherence of the spiral but would decrease the peak intensities. The second term in Eq. (18) distributes intensity into diffuse peaks displaced by $(00\pm\delta)$ from each $\vec{G}$. These peaks have the same halfwidth as $S(\vec{K})$ which is approximately the same as their displacement from $\vec{G}$ [see Fig. 7(b)]. The x and y domains also produce such peaks displaced by $(\pm\delta00)$ and $(0\pm\delta0)$ and the net result is a broad peak centered at each $\vec{G}$. At (000) for the 25-at.% Mn alloy we calculate 0.31 b arising from this $S(\vec{K}\pm\vec{Q}_M)$ term. An additional 0.14 b is contributed by the terms in Eq. (13). The total of 0.45 b

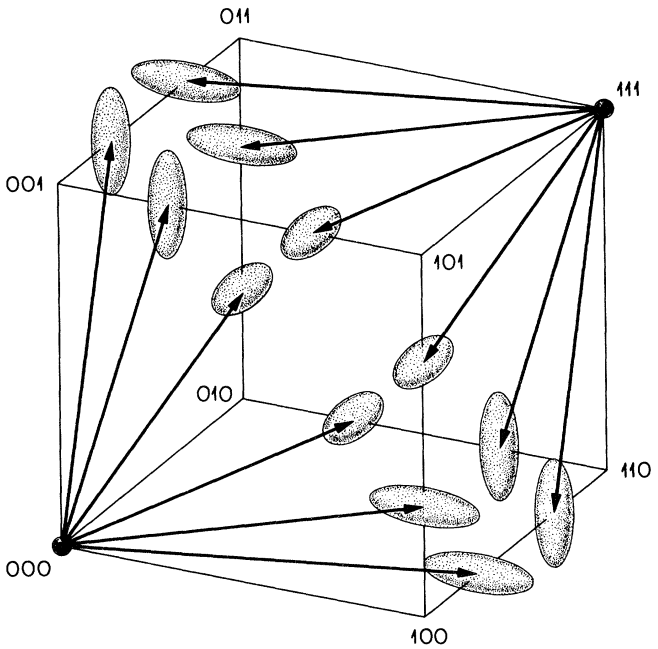

FIG. 10. Schematic representation of the symmetry and relative orientations of the $(1,0,\frac{1}{2}\pm\delta)$-type diffuse peaks in the reciprocal lattice. Each of the $\vec{Q}_M$ radiating from (000) corresponds to a single domain and has an equivalent $-\vec{Q}_M$ radiating from (111).

compares favorably with the "observed" value of 0.5 b obtained by extrapolation of an $(h00)$ scan.

Thus, the assumed spin correlations account for all of the observed magnetic scattering. The $(1,0,\frac{1}{2}\pm\delta)$ peaks are from an incommensurate long-period modulation and the broad peaks at $(1\,0\,\frac{1}{2})$ arise from short-range spin correlations that are directly associated with the atom pair correlations. In the concentrated region only the convolution terms between the spin and atomic correlations give rise to the diffuse peaks at $\vec{G}$.

CONCLUSIONS

The microscopic spin structure for Cu-Mn alloys that emerges from these considerations is basically an incommensurate long-period modulation. This is not a simple modulation in the sense that antiparallel alignment is required for nearest-neighbor spins in the plane normal to the modulation direction. Stabilization of such a structure over such a large concentration region probably requires a long-range interaction such as the Rudderman-Kittel-Kasuya-Yosida interaction via the conduction electrons. The variation in the period of the modulation from approximately $6a_0$ at 5 at.% Mn to about $3a_0$ at 25 at.% Mn would then be attributed to the change in k_F with increasing Mn content. Although long-range order does not develop, this modulation occurs over large volumes in real space with a Gaussian correlation length of $2/\sigma \simeq 6a_0$. This corresponds to short-range-ordered regions containing approximately 2000 atoms, of which the fraction c are Mn atoms.

According to the model proposed here, this is the only type of spin order that would occur if these were random alloys. However, additional spin correlations develop in the presence of atomic short-range order. At low Mn concentrations these are ferromagnetic correlations within the short-range-ordered regions, while at higher Mn concentrations these have the same signs and approximately the same range as the atom pair correlations. For Mn-Mn pairs, this produces fewer than the average number of Mn first neighbors (which align antiparallel) and more than the average number of Mn second neighbors (which align parallel). This results in ferromagnetic regions with dimensions defined by the range of the atomic short-range order. The observed Gaussian correlation lengths yield short-range ferromagnetic regions with average volumes containing about 20 atoms at 5 at.% Mn up to about 50 atoms at 25 at.% Mn. Since both sets of peaks have intensities proportional to c^2 (Fig. 7), these small ferromagnetic regions coexist homogeneously with the much larger modulated regions where they locally perturb the modulation without destroying its coherence.

The magnetic configurations inferred from the polarization-analysis experiments described in this paper are consistent with the ferromagnetic-antiferromagnetic models discussed by Kouvel[4] and Beck.[5] However, the incommensurate nature of the antiferromagnetism and the intimate connection of the ferromagnetism with the atomic short-range order could not have been anticipated. The susceptibility cusp at T_f and the anisotropic energy barriers below T_f may well arise from freezing of the ferromagnetic regions into directions defined by the local interactions with the incommensurate modulated regions. This freezing is not observed in the present experiment, because the energy resolution is sufficiently broad to accept the total elastic and inelastic scattering. We are planning high-resolution inelastic scattering and small-angle scattering experiments to probe the microscopic origin, in space and time, of the freezing mechanism.

ACKNOWLEDGMENTS

This research was sponsored by the Division of Materials Science, U. S. Department of Energy, under Contract No. W-7405-eng-26 with the Union Carbide Corporation.

*Present address: Department of Physics, Keio University, Yokohama 223, Japan.

[1]S. Valentiner and G. Becker, Z. Phys. 80, 735 (1933).
[2]E. Scheil and E. Wachtel, Z. Metallkd. 48, 571 (1957).
[3]D. Meneghetti and S. S. Sidhu, Phys. Rev. 105, 130 (1957).
[4]J. S. Kouvel, J. Phys. Chem. Solids 21, 57 (1961).
[5]P. A. Beck, Prog. Mater. Sci. 23, 1 (1978).
[6]J. A. Mydosh, J. Magn. Magn. Mater. 7, 237 (1978).
[7]A. P. Murani, J. Magn. Magn. Mater. 5, 95 (1977).
[8]A. P. Murani and J. L. Tholence, Solid State Commun. 22, 25

(1977).
[9]A. P. Murani, Phys. Rev. Lett. 41, 1406 (1978).
[10]A. P. Murani and A. Heidemann, Phys. Rev. Lett. 41, 1402 (1978).
[11]F. Mezei and A. P. Murani, J. Magn. Magn. Mater. 14, 211 (1979).
[12]A. P. Murani, Solid State Commun. 33, 433 (1980).
[13]A. P. Murani, J. Magn. Magn. Mater. 22, 271 (1981).
[14]S. Schultz, E. M. Gullikson, D. R. Fredkin, and M. Tovar, Phys. Rev. Lett. 45, 1508 (1980).
[15]E. M. Gullikson, D. R. Fredkin, and S. Schultz, Phys. Rev. Lett. 50, 537 (1983).
[16]B. I. Halperin and W. M. Saslow, Phys. Rev. B 16, 2154 (1977).
[17]W. M. Saslow, Phys. Rev. B 22, 1174 (1980).
[18]W. M. Saslow, Phys. Rev. Lett. 48, 505 (1982).
[19]P. Wells and J. H. Smith, J. Phys. F 1, 763 (1971).
[20]J. R. Davis, S. K. Burke, and B. D. Rainford, J. Magn. Magn. Mater. 15-18, 151 (1980).
[21]H. Sato, S. A. Werner, and M. Yessik, in *Magnetism and Magnetic Materials—1971 (Chicago),* Proceedings of the 17th Annual Conference on Magnetism and Magnetic Materials, edited by D. C. Graham and J. J. Rhyne (AIP, New York, 1972), p. 508.
[22]S. A. Werner, H. Sato, and M. Yessik, in *Magnetism and Magnetic Materials—1972 (Denver),* Proceedings of the 18th Annual Conference on Magnetism and Magnetic Materials, edited by C. D. Graham and J. J. Rhyne (AIP, New York, 1973), p. 679.
[23]N. Ahmed and T. J. Hicks, Solid State Commun. 15, 415 (1974).
[24]N. Ahmed and T. J. Hicks, J. Phys. F 5, 2168 (1975).
[25]J. R. Davis and T. J. Hicks, J. Phys. F 9, 753 (1979).
[26]In abbreviated form, S. A. Werner and J. W. Cable, J. Appl. Phys. 52, 1757 (1981); J. W. Cable, S. A. Werner, G. P. Felcher, and N. Wakabayashi, Phys. Rev. Lett. 49, 829 (1982).
[27]J. M. Sanchez and D. de Fontaine, Phys. Rev. B 21, 216 (1980).
[28]M. Hirabayashi, M. Koiwa, S. Yamaguchi, and K. Kamata, J. Phys. Soc. Jpn. 45, 1591 (1978).
[29]H. Bouchiat, E. Dartyge, P. Monod, and M. Lambert, Phys. Rev. B 23, 1375 (1981).
[30]A. Mukhopadhyay and P. A. Beck, Solid State Commun. 16, 1067 (1975).
[31]A. K. Mukhopadhyay, R. D. Shull, and P. A. Beck, J. Less-Common Metals 43, 69 (1975).
[32]R. W. Tustison, Solid State Commun. 19, 1075 (1976).
[33]R. W. Tustison and P. A. Beck, Solid State Commun. 20, 841 (1976).
[34]W. Marshall and S. W. Lovesey, *Theory of Thermal Neutron Scattering* (Oxford University Press, Oxford, 1971), p. 111.